

# Non-intrusive Water Flow Rate Measurement: A TEG-powered Ultrasonic Sensing Approach

Domenico Balsamo<sup>1\*</sup>, Oktay Cetinkaya<sup>2</sup>, Sergey Mileiko<sup>1</sup>

<sup>1</sup>MicroSystems Research Group, School of Engineering, Newcastle University, Newcastle NE1 7RU, UK.

<sup>2</sup>Oxford e-Research Centre, Department of Engineering Science, University of Oxford, Oxford OX1 3QG, UK.

\*domenico.balsamo@newcastle.ac.uk

**Abstract**—This paper proposes a thermoelectric generator (TEG)-powered ultrasonic sensing system for non-intrusive water flow rate measurement. The limited power provided by the TEGs is handled by a dedicated energy management unit (EMU), allowing reliable sensing, computation, and transmission tasks. First, we introduce the delta time-of-flight ( $\Delta ToF$ )-based ultrasonic sensing and thermoelectric energy generation theory. Then, the design is given, followed by the system evaluation under different harvesting conditions to show their impact on average sensing and transmission times. The results revealed that our method could achieve high measurement accuracy ( $\pm 1.4\%$ ), comparable to intrusive and battery-powered counterparts, thereby offering a “plug&play+deploy&forget” hybrid solution.

**Index Terms**—Non-intrusive, ultrasonic sensors, delta time-of-flight, water flow rate measurement, thermoelectric generators.

## I. INTRODUCTION

Conventional methods for water flow rate measurement have a long-run trade-off between non-intrusiveness, the autonomy of energy/operation, and ease of deployment/maintenance. To be precise, the meters protruding into the water offer self-sufficiency but require skilled personnel for installation [1]. On the other hand, the *clamp-on* counterparts relieve that drawback at the cost of being battery- or mains-powered [2]. This confirms that the field looks forward to a non-intrusive and autonomous solution, which this paper aims to accomplish.

Non-intrusive measurement requirement can be fulfilled by ultrasonic sensors, which transmit high-frequency pulses penetrating the pipes and propagating through the water. The difference between the propagation times of these pulses, i.e., delta time-of-flight ( $\Delta ToF$ ), is used to measure the water flow rate [3]. For energy autonomy, thermoelectric generators (TEGs) can be used to harvest energy from the temperature gradients between pipes and the medium they reside [4].

Despite sounding straightforward, it is not that easy to adapt these components together. The main bottleneck when using TEGs is that they generate much less power than is required to perform ultrasonic signal acquisition,  $\Delta ToF$  calculation, and data transmission uninterruptedly. Hence, a dedicated energy management unit (EMU) is needed to handle these operations as a function of the harvested power by storing charges up to predefined energy levels required by each operation [5].

In the light of these, this paper proposes a TEG-powered ultrasonic sensing system underpinned by a dedicated EMU for non-intrusive water flow rate measurements (Sec. III). We

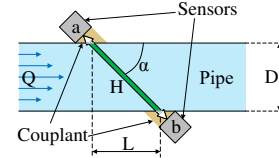


Figure 1: Non-intrusive ultrasonic sensors measuring the flow rate,  $Q$ .

evaluated our system under various harvesting conditions and showed their effect on signal acquisition and transmission times (Sec. IV). The results revealed that our design could achieve high measurement accuracy (1.4%), comparable to its intrusive and battery-powered counterparts. Thus, it stands quite promising as a non-intrusive and autonomous alternative.

## II. THEORETICAL OVERVIEW

This section overviews the  $\Delta ToF$ -based ultrasonic sensing and the thermal energy harvesting (EH) theory, including the practical design aspects.

### A. Ultrasonic Water Flow Rate Measurement Theory

Fig. 1 illustrates how to measure water flow rate,  $Q$ , with non-intrusive ultrasonic sensors based on the  $\Delta ToF$  technique. Two sensors,  $a$  and  $b$ , are vis-a-vis placed on a pipe of diameter  $D$ , with separation of  $L$  along the pipe axis. When the ultrasonic pulse propagates through the flowing water, the time it takes from  $a$  to  $b$ , and  $b$  to  $a$ , varies with flow velocity. The flight times of the upstream ( $UPS$ ) and downstream ( $DNS$ ) pulses/signals,  $t_{UPS}$  and  $t_{DNS}$ , can be expressed as:

$$t_{UPS} = \int_0^H \frac{dh}{v_w - v(h) \cos \alpha} \text{ and } t_{DNS} = \int_0^H \frac{dh}{v_w + v(h) \cos \alpha}, \quad (1)$$

where  $H$  is the acoustic path length,  $v_w$  is the velocity of the ultrasonic wave propagating in steady water,  $\alpha$  is the angle between sensors and the pipe, and  $v(h)$  is the axial flow velocity measured at an arbitrary point  $h$  along  $H$ .

As shown in Fig. 2, the difference between flight times, i.e.,  $t_{UPS} - t_{DNS}$ , given in (1) defines the  $\Delta ToF$ . Hence,  $v$  can be obtained in terms of  $\Delta ToF$  assuming that it is independent of  $h$ , and  $v_w \gg v$  [6]:

$$v = v_w^2 \frac{\Delta ToF}{2L}. \quad (2)$$

The water flow rate,  $Q$ , is the product of  $v$  and the cross-sectional area of pipe,  $A$  ( $= \pi D^2$ ), i.e.,  $Q = vA$ . However,

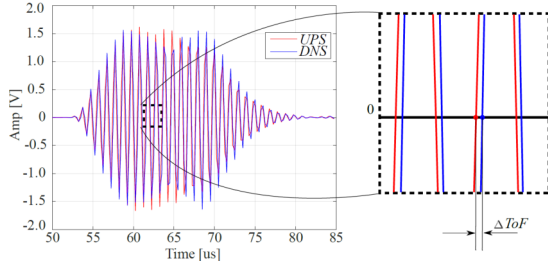


Figure 2: Received *UPS* and *DNS* signals and the  $\Delta ToF$ .

$v_w$  is affected by the chemical composition, temperature, and impurities of/in the water. Also, due to the non-intrusive nature of the measurement, it is challenging to determine the actual value of  $v_w$  and so the  $\Delta ToF$ . Hence, this study uses a *cross-correlate then interpolate* method for calculating the  $\Delta ToF$ , while the linear relationship between the calculated  $\Delta ToF$  and  $Q$  is determined empirically [3]. This method measures the similarity between *UPS* and *DNS* signals as a function of the displacement of one relative to the other as below:

$$Corr(k) = \sum_{i=1}^N UPS_{i+k} DNS_k, \quad k = \{-m, -m+1, \dots, 0, \dots, m-1, m\},$$

where  $N$  is the total number of samples. In practice, this function shifts *UPS* along the x-axis (equal to the sampling rate), thereby calculating the integral of the product of *UPS* and *DNS* at each position. When *UPS* and *DNS* match, *Corr* is maximized; therefore, the value of  $\Delta ToF$  is proportional to the shift between  $Corr(0)$  and  $max(Corr)$ . Since *UPS* and *DNS* are sampled at a low rate due to the limitations of the platform used, it is not possible to calculate the exact  $\Delta ToF$  directly. To overcome this issue, the resultant signal of the *Corr* function is interpolated to construct additional points within the range of a discrete set of the known points.

### B. Thermoelectric Energy Harvesting Theory

The TEGs' harvesting capability is based on the Seebeck effect that generates electrical energy from the temperature difference between the two surfaces of a Peltier cell [7]. The power is harvested from the heat flow  $q$  through the surfaces with efficiency  $\eta$ , i.e.,  $P_h = \eta \cdot q$ . The heat flows from the water (with temperature  $T_w$ ) to the environment (with temperature  $T_{env}$ ), considering hot water circulating in the pipe. The value of  $q$  is proportional to the temperature difference between the water and environment,  $\Delta T = T_w - T_{env}$ , and the thermal conductivity  $\Theta$  of the path between them,  $q \propto \Delta T \cdot \Theta$ , while  $\eta$  depends on multiple factors, including the temperature drop over the TEG, the internal resistance, and the load [8, 9].

The main factor limiting the heat flow is the thermal exchange between the colder side of the TEG and the environment; the larger the contact area, the higher  $\Theta$ . However, increasing the contact area can be done to a certain extent. As depicted in Fig. 3, we use heatsinks to increase  $\Theta$  between the cold side of the TEG by enlarging the contact area with the environment. Based on this,  $\Theta$  is given by the sum of the thermal conductivity of the TEG and heatsink,  $\Theta = \Theta_{TEG} + \Theta_{hs}$ .

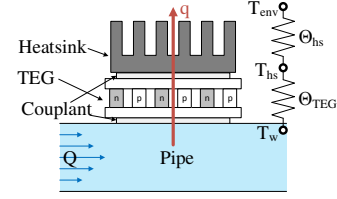


Figure 3: Thermal energy harvester placed on a pipe.

In opposition to the increased  $\Theta$ , a heatsink with high  $\Theta_{hs}$  has a higher temperature drop,  $\Delta T_{hs} = T_{hs} - T_{env}$ , limiting the temperature drop across the TEG,  $\Delta T_{TEG} = T_w - T_{hs}$ , resulting in a lower efficiency  $\eta$ , which can be expressed as:

$$\eta \propto \frac{\Delta T_{TEG}}{\Delta T_{TEG} + \Delta T_{hs}}. \quad (3)$$

Previous studies demonstrated that the optimal trade-off is obtained when the thermal conductivity value is  $\Theta_{TEG} = \Theta_{hs}$ , implying that  $\Delta T_{TEG} = \Delta T_{hs}$  [4]. The main factor affecting the values of  $\Theta_{TEG}$  and  $\Theta_{hs}$  is the size of the TEG and the heatsink. A larger size means a higher  $\Theta$ ; hence, more power harvested. However, the TEG size is limited by the pipe since the thermal exchange between them is required. This limitation was crucial for selecting a TEG and a heatsink for our design.

From the electrical viewpoint, the EH efficiency can be increased by matching the load resistance connected to the TEG with the TEG's internal resistance ( $R_{TEG}$ ). The value of  $R_{TEG}$  does not change significantly with the variations of  $\Delta T_{TEG}$  within the range of temperatures considered for water distribution applications. As a result, an advanced technique for variable power sources is not required to maximize the energy extraction [7]. Note that, although we considered hot water, the same applies to water colder than the environment.

### III. SYSTEM DESIGN

Fig. 4 shows the energy and control flows between the three main components of the system: a) the two TEGs harvesting energy from both cold and hot water, b) the EMU managing the harvested energy and providing the supply voltage for c) the load. Depending on the next task to be executed (sensing *UPS/DNS* and calculating  $\Delta ToF/Q$  or data transmission), the load configures the supply voltage before shutdown, and controls the EMU, as shown with the dashed line in Fig. 4. The EMU stores the required energy through an internal capacitor,  $C_{store}$ . When  $C_{store}$  is charged to the energy level defined by  $V_{load}$ , the EMU produces the power needed to drive the load.

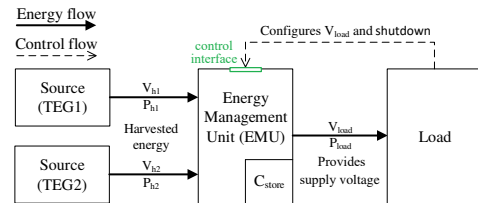


Figure 4: System design and the flows between its components.

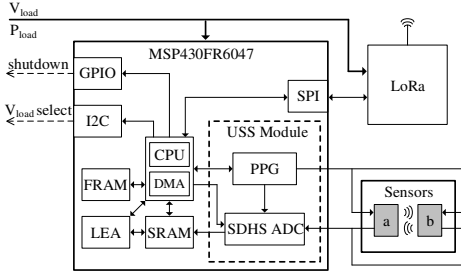


Figure 5: Schematic of the ultrasonic sensor controller, i.e., the load.

### A. Ultrasonic Sensor Controller

As shown in Fig. 5, the load has an MSP430FR6047 [10] microcontroller unit (MCU) consisting of an ultrasonic sensing (USS) module designed for ultrasonic measurements. The USS module includes a programmable pulse generator (PPG) and a sigma-delta high-speed (SDHS) analogue-to-digital converter (ADC). The PPG generates the electric train of pulses for the ultrasonic sensors [11] and transforms these into ultrasonic signals, i.e., *UPS* and *DNS*. The SDHS ADC captures these signals and stores them in SRAM without CPU intervention. The MCU also includes a low energy accelerator, for the computation-intensive operations, e.g., cross-correlation and interpolation. The MCU uses the SPI to communicate with the LoRa module [12] and I2C interface to configure the EMU (set  $V_{load}$ ) or request the shutdown when the tasks are completed.

### B. Sensor Operations

Once the EMU collects the energy required, the system first performs  $M$  measurements, each of which includes *UPS* and *DNS* samplings. Afterwards, *min*, *max*, and *average* values of  $\Delta ToF$  are calculated and saved in FRAM before sending a shutdown request. This turns the load off until the next energy level is reached. When this happens, the system configures the LoRa module and transmits a packet consisting of the  $\Delta ToF$  values saved in FRAM. When the transmission is completed, a new shutdown request is sent, restarting the cycle. Tab. I presents the experimentally measured energy costs of the tasks: *i*) sensing *UPS/DNS* and calculating  $\Delta ToF/Q$ , and *ii*) data transmission. Here,  $E_{ton}$  is the energy required to turn on the system,  $E_{conf}$  to configure it, and  $E_{shdn}$  to shut it down.  $E_{meas}$  is the energy consumed for a single measurement, and  $E_{tran}$  if for data transmission;  $t_{exec}$  is the execution time. From these parameters,  $C_{store}$  was calculated to accommodate task *ii*), resulting in  $C_{store} = 0.69\text{mF}$  with  $M = 5$  per cycle.

## IV. EXPERIMENTAL RESULTS

Fig. 6 illustrates how charging time for  $C_{store}$  and measurement period is affected by  $\Delta T$  between the pipe and the

Table I: System parameters.

Task	$E_{ton}$ (mJ)	$E_{conf}$ (mJ)	$E_{shdn}$ (mJ)	$E_{meas}$ (mJ)	$E_{tran}$ (mJ)	$C_{store}$ (mF)	$t_{exec}$ (ms)
<i>i</i> )	0.41	0.21	0.02	0.032	-	-	55
<i>ii</i> )	0.69	0.3	0.03	-	2.11	0.69	46

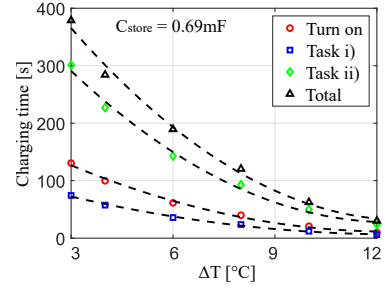


Figure 6: Time to turn on, *task i*) and *task ii*), and period between measured data vs  $\Delta T$  between water in the pipe and the environment.

environment. To be more specific, it shows the  $C_{store}$  charging time to reach the turn-on point, to build-up the energy for *task i*) and *task ii*), and the period between measurements, including both measurement and transmission tasks. The results demonstrate that the system can take and transmit measurements every 30sec at a  $\Delta T$  of  $12^\circ\text{C}$ . This duration extends to 6min when  $\Delta T$  drops to  $3^\circ\text{C}$ . For  $\Delta T$  values lower than  $3^\circ\text{C}$ , the system stops harvesting energy since the voltage generated by the TEGs is not enough to drive the EMU. This level, i.e., the minimum  $\Delta T$  value for system operation, can be further reduced by improving the thermal connectivity between the heatsink and the environment.

Finally, Fig. 7 provides the water flow rate measurement results when the ultrasonic sensors are placed on pipes of varying materials and diameters. The best precision is achieved when the sensors are placed on a 15mm copper pipe, which is  $\pm 1.4\%$ . This is thanks to averaging  $\Delta ToF$  values based on multiple measurements,  $M$ , allowing an accuracy comparable to intrusive or battery-powered meters available on the market.

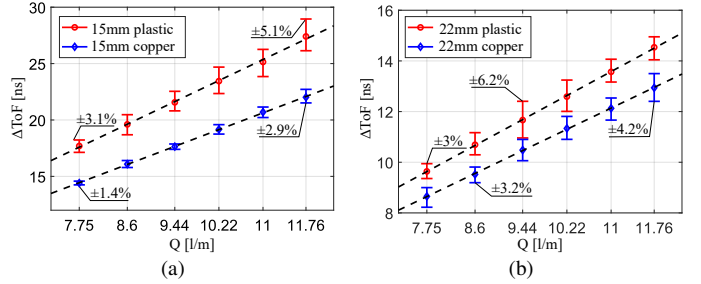


Figure 7:  $\Delta ToF$  vs.  $Q$  for sensors placed on (a) 22mm copper and 22mm PVC, and (b) 15mm copper and 15mm PVC pipes.

## V. CONCLUSIONS

This paper presents a TEG-powered ultrasonic sensor system for non-intrusive water flow rate measurement. After the theoretical overview of signal acquisition and thermal EH, system design is provided. The empirical results demonstrated a high level of precision in the flow rate values achieved by our system, which is comparable to its off-the-shelf counterparts.

## VI. ACKNOWLEDGMENT

This work was supported by EPSRC Grant EP/R511584/1 (IAA). The authors would like to thank Chris Jones, David Scott, and Carl Samuel for their invaluable support.

## REFERENCES

- [1] X. Li and P. Chong, "Design and implementation of a self-powered smart water meter," *Sensors*, vol. 19, p. 4177, 2019.
- [2] M. Arsalan, "Advances in Clamp-On Flow Measurement Techniques," *Abu Dhabi International Petroleum Exhibition and Conference*, 2020.
- [3] S. Mileiko *et al.*, "A non-intrusive ultrasonic sensor system for water flow rate measurement," *2021 IEEE Sensors Applications Symposium (SAS)*, pp. 1–6, 2021.
- [4] G. J. Snyder, *Energy Harvesting Technologies*. Springer US, 2009, ch. Thermoelectric energy harvesting, pp. 325–336.
- [5] A. Gomez *et al.*, "Dynamic energy burst scaling for transiently powered systems," *2016 Design, Automation & Test in Europe Conference & Exhibition (DATE)*, pp. 349–354, 2016.
- [6] Y. Chen *et al.*, "Acoustic propagation in viscous fluid with uniform flow and a novel design methodology for ultrasonic flow meter," *Ultrasonics*, vol. 53, no. 2, pp. 595–606, 2013.
- [7] L. J. Bierschen, *Energy Harvesting Technologies*. Springer US, 2009, ch. Optimized Thermoelectrics For Energy Harvesting Applications, pp. 337–351.
- [8] M. H. Cobble, *Calculations of Generator Performance*. New York: SCRC Press, 1995.
- [9] M. Freunek *et al.*, "Modified model for thermoelectric generators," *Tc*, vol. 3, p. 4, 2008.
- [10] "Msp430fr6047 microcontroller datasheet," <https://www.ti.com/product/MSP430FR6047>, accessed: 2022-07-01.
- [11] "Ultrasonic flow transducers jiakang electronics," <http://en.jkelec.com/index.php?c=content&a=show&id=405>, accessed: 2022-07-01.
- [12] "Transceiver hoperf rfm95 datasheet," <https://www.hoperf.com/modules/lora/RFM95.html>, accessed: 2022-07-01.